Research Article

Xiaofei Teng*, Ping Tan, Dewen Liu, Linli Zhou, Jianmin Jin, Huating Chen, and Yanhui Liu

Influence of different seismic motion input modes on the performance of isolated structures with different seismic measures

https://doi.org/10.1515/phys-2020-0140
received November 07, 2019; accepted April 22, 2020

Abstract: In order to obtain the influence of different seismic motion input modes on the performance of isolated structures with different seismic measures, the two aspects from near-fault seismic motion velocity pulse input and different dimension seismic motion input modes are studied. The finite element model of traditional seismic and base isolation frame structure with different aspect ratios is established. The actual near-seismic strong earthquake record with forward directional effect and slipping speed pulse is used as the input method of structural seismic motion to carry out nonlinear dynamics. The different dimensional seismic motion input method is selected as the quantitative, the tensile–compression stiffness ratio is the variable, and the time-history analysis of the isolation performance of a high-rise isolated structure is carried out. The experimental results show that for structures with an aspect ratio H/B of 1, 2, 3, and 4, the smaller the aspect ratio is, the better the damping effect is; the different dimensional vibration input has less isolation performance for the isolation bearing. From small to large, it is: one-dimensional vibration input, two-dimensional vibration input, three-dimensional vibration input.

Keywords: vibration input, seismic measures, near-fault, isolated structure, time-history analysis, aspect ratio

*** Corresponding author: Xiaofei Teng,** Department Architecture and Civil Engineering, School of Civil Engineering of Jiaying University, Meizhou 514021, China, e-mail: afeiteng538@sina.com
Ping Tan, Linli Zhou, Jianmin Jin, Huating Chen, Yanhui Liu: Engineering Seismic Analysis Laboratory, Earthquake Engineering Research & Test Center, Guangzhou University, Guangzhou 510405, China
Dewen Liu: Department of Civil Engineering, College of Civil Engineering, Southwest Forestry University, Kunming 650000, China

1 Introduction

Earthquakes can release huge amounts of energy and cause strong damage to buildings, especially tall buildings. The emergence of isolation technology has made the building structure more resistant to earthquakes [1,2]. The isolation can concentrate the deformation of the structure on the isolation layer, prolong the natural vibration period of the structure, and reduce the acceleration of the isolation structure, thereby reducing the reaction of the upper structure and achieving the purpose of damping.

Japan is currently the country with the best development of isolation technology, and it has the largest number of isolated structures. The development of isolation technology in the United States is also a world leader, and its isolated buildings are mainly concentrated in the California area [3–5]. In addition, the isolation technology in countries, such as Italy, New Zealand, and Armenia, has a fairly advanced level of development. Seismic isolation technology has become one of the effective means of seismic and shock absorption of high-rise structures with its excellent shock absorption effect, safety and applicability, and has been widely promoted and applied [6]. China's research on isolation technology started in the early 1990s, and then experienced a gradual development period, and achieved rapid development after the Wenchuan earthquake. In the Ya'an earthquake in 2010, only the Lushan County Lushan People's Hospital with isolated construction technology remained intact, which further aroused people's attention and research on isolated building technology. Up to now, China's research and application of isolation technology has been relatively mature, and has gradually become an important structural vibration control technology.

In recent decades, several major earthquakes at home and abroad have brought enormous disasters and losses to human beings, such as the 1994 Northridge earthquake in Los Angeles, the 1999 earthquake in Taiwan, China, and the Wenchuan earthquake in China in 2008. The near-fault seismic motions of the above earthquakes show significant

velocity pulse characteristics [7,8]. Near-fault velocity pulse-type seismic motion is more concentrated and more destructive in a shorter seismic motion period than a seismic motion without a velocity pulse [9]. Therefore, the engineering structure under near-fault velocity pulse type ground motion and ground motion without velocity pulse, especially the seismic response under the vibration of the COSCO field, will be very different.

In addition, due to the influence of the traditional seismic design, most of the existing researches on seismic isolation design are only on horizontal seismic motion, and little attention is paid to the influence of the vertical component of seismic motion on the structure [10]. However, a large number of seismic field survey results show that the vertical component of seismic motion is not negligible, and even exceeds the horizontal component in the vicinity of the epicenter. Therefore, for the study of seismic isolation design, the vertical component of seismic motion cannot be ignored. In addition, it has been confirmed by research that the tensile–compression stiffness ratio of the isolation bearing is different, but the result only considers the effect of the horizontal earthquake, and the different responses of the isolated structure under the vertical earthquake are not analyzed [11,12].

On the one hand, the paper studies the problem of the performance of the isolated structure for different seismic measures. On the other hand, the article uses the aspect ratio of the isolated structure as the main variation parameter and selects the lead laminated rubber bearing as the isolation device [13]. Using the finite element analysis software MIDAS-GEN, four traditional seismic frame structures and four corresponding base isolation structures are established. Six near-fault seismic motion records with typical velocity pulse characteristics are selected as the structural seismic motion input, to make structural nonlinear dynamic time-history analysis [14,15]. The seismic responses of traditional seismic structures and base isolation structures with different aspect ratios under near-fault velocity pulse-type ground motion are compared. The influence of velocity pulses on the isolation effect of isolation structures with different aspect ratio bases is analyzed. The appropriate aspect ratio of the base isolation structure in the fault zone is discussed.

On the other hand, based on the seismic motion input dimension as a variable, the different responses of the isolated structures under different dimensional seismic motion inputs are compared and analyzed [16–18]. Then, the tensile–compression stiffness ratios of the isolation units are used as variables to study different tensile–compression stiffnesses. The variation of the surface pressure of the isolated base and its variation law are studied to examine the influence of different dimensional seismic motion input methods on the isolation performance of the isolated structure.

2 Materials and methods

2.1 Influence of near-fault seismic motion velocity pulse input on the isolation performance of base isolation structures with different aspect ratios

In order to consider the influence of velocity pulses on the structural response of different generation mechanisms, six near-fault velocity pulse seismic motion records are selected as inputs, including three forward directional effect velocity pulse types of seismic motion records (A1, A2, A3) and three slipping effect speed pulse types of seismic motion records (B1, B2, B3). Table 1 shows the relevant parameters of the selected seismic motion record, wherein the strong earthquake holding time is the corresponding time of the peak acceleration with an amplitude greater than 10%.

Taking the framework structure as the analysis object, the structural response calculation is carried out using the finite element analysis software MIDAS-GEN [19]. In order to facilitate the comparative analysis, all the models are arranged in the same plane, with a structural plane length of 36 m and a width of 14.4 m and a standard layer height of 2.9 m. *X*-Directional is 5 span, the span degree is 7.2 m, *Y*-directional is 3 span, the span degrees are 6.0, 2.4, and 6.0 m, respectively. When the width of all models is the same, by changing the height of the structure, a traditional seismic frame structure model with an aspect ratio H/B of 1, 2, 3, and 4 (5, 10, 15, and 20 floors, respectively) and the corresponding base isolation structure model are established. In order to better study the influence of the aspect ratio on the isolation system, the analysis models in this paper keep the overall height of the building unchanged, but change the width to get a structure with different aspect ratio. H represents the total height of the model and B represents the width of the model.

When establishing the model, by considering the following construction site environment: the basic wind pressure is 0.45 kN/m^2, the basic snow pressure is 0.4 kN/m^2, the ground roughness is Class C, the environmental category is Class II, and the fortification intensity is 7. The designed basic seismic acceleration is 0.10 g. The roof is a non-superman roof with a constant load of 2.5 kN/m^2 and a live load of 0.5 kN/m^2. The floor constant load is 2 kN/m^2 and the live load is 2 kN/m^2;

Table 1: Relative parameters of the near-fault velocity pulse seismic motion record

Generation mechanism	Directional effect			Slippery effect		
Seismic number	**A1**	**A2**	**A3**	**B1**	**B2**	**B3**
Magnitude	7.1	6.5	6.5	7.6	7.6	7.6
Station	Newhall-W. Pico Canyon	Rd E07	UCSC station 16	TCU75	TCU76	TCU129
Weight	46	sn	—	EW	EW	EW
A_{max}/(cm s^{-2})	445.9	453.71	563.1	340.51	325.27	496.73
V_{max}/(cm s^{-1})	92.8	109.27	94.8	116.21	69.1	68.2
V_{max}/A_{max}/s	0.208	0.241	0.172	0.341	0.212	0.137
t/s	11	14	25	35	38	38
Δt/s	0.01	0.01	0.005	0.01	0.01	0.01

Table 2: Main construction dimensions of structural models

Model number	H/B	Total number of layers	Column section		Beam section in *x* direction		Beam section in *y* direction	
			b_c/mm	h_c/mm	b_{b1}/mm	h_{b1}/mm	b_{b2}/mm	h_{b2}/mm
RC1	1	5	600	600	250	600	300	600
RC2	2	10	800	800	400	600	400	600
RC3	3	15	1,000	1,000	300	600	400	600
RC4	4	20	1,200	1,200	300	600	400	600

the linear load of decoration tiles on beams is 5.5 kN/m^2 and the linear load of parapet wall on top beams is 2.5 kN/m^2. C30 is used in concrete, HRB400 is used in reinforcing bars, and HPB300 model is used in stirrup design, mainly according to the corresponding codes and regulations. The main component size of the structural model is shown in Table 2.

Based on the traditional seismic structure model, the base isolation structure model is provided with an isolation device under each column of the bottom layer. Lead-core rubber isolation bearings are used to reduce the natural frequency of the structure after the lead yielding and to avoid the structural resonance effect to achieve the isolation effect [20]. According to the provisions of GB 50011-2010, the horizontal displacement limit of the isolation bearing should be 0.55 times greater than its effective diameter and 3 times the total rubber thickness of the bearing. After calculation, for the isolation structure model with an aspect ratio of 1, 2, 3, and 4, the lead rubber bearing of GZY400, GZY600, GZY800, and GZY1000 models is selected as the isolation device in turn. The main parameters of the lead rubber bearing are shown in Table 3. Figure 1 shows a three-dimensional model of a base-isolated structure with an aspect ratio of 2. Analysis of Figure 1 shows the structure of the building structure with an aspect ratio of 2. The black dot O in the figure represents the isolation device under the columns on the ground and the bottom of the building, where *X*, *Y*, and *Z* represent the lateral, longitudinal, and vertical directions of the building structure, respectively. *X* is also the column of the building structure. The force rod adopts different lengths based on the structure of each layer. Based on the structure of Figure 1, the experimental research is carried out in combination with the parameters given in Table 3.

The peak accelerations of the six seismic motion records were adjusted to 220 cm/s^2, which is a rare seismic motion

Table 3: Parameters of lead rubber bearing

Category	d_e/mm	h_{total}/mm	K_v/(kN mm^{-1})	K_y/(kN mm^{-1})	F_y/kN
GZY400	400	68.6	1,750	788	42.7
GZY600	600	110	2,900	1,106	96.08
GZY800	800	160	4,400	1,693	170.82
GZY1000	1,000	162	6,900	2,086	266.9

Note: d_e is the effective diameter; h_{total} is the total thickness of the rubber layer; K_v is the vertical stiffness; K_y is the post-yield stiffness; F_y is the yielding force.

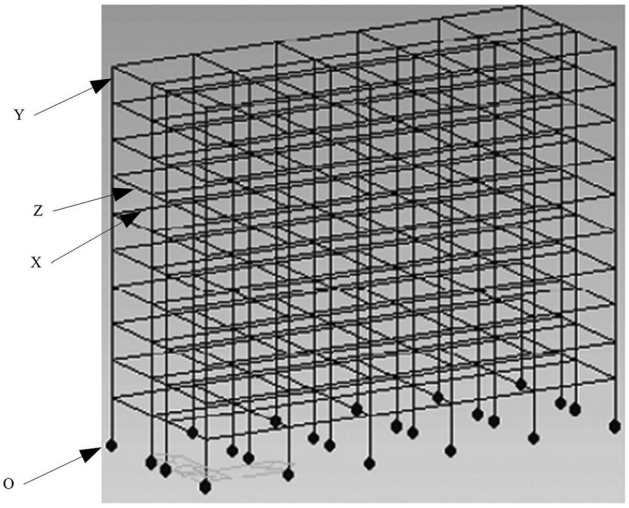

Figure 1: Three-dimensional model of the basic isolation structure with an aspect ratio of 2.

with 7 degrees. For the dynamic elastoplastic analysis of the model structure, the Newmark method [21] in the direct integration method is used for calculation.

In the analysis model, the traditional seismic structures with an aspect ratio of 1–4 have first-order natural vibration periods of 0.51, 0.98, 1.56, and 2.21 s, respectively; the first-order natural vibration periods of the corresponding base-isolated structures are: 2.03, 2.99, 3.72, and 3.87 s, respectively.

2.2 Study on the influence of different dimensional seismic motion input methods on the isolation performance of seismic isolation bearings

By analyzing the tensile–compression stiffness ratio of different dimensional seismic motion inputs to the isolation bearing, the influence of different dimensional seismic motion inputs on the isolation performance of the isolated bearing is studied.

2.2.1 Project overview

Seismic analysis is carried out with a high-rise building structure as the research object. The total height of the building is 60 m, excluding the isolation layer, the lateral width is 33.6 m, the longitudinal length is 42 m, the aspect ratio is about 1.8, the total is 14 layers, the height of the first layer is 6 m, the second layer is 5.7 m, and the 3–14th layers is 5 m. The structural system of the building is frame-core tube and the structure damping ratio is 5%. The building classification is C-class, the structural design has a service life of 50 years, the site category is class II, the fortification intensity is 8 degrees, and the designed peak value of basic seismic acceleration is 0.3 g. The design of earthquake group is the first group and the site characteristic period is 0.35 s.

2.2.2 Simulation of isolation bearing

At present, the software that can be used for the time-history analysis of isolated structures is SAP2000,

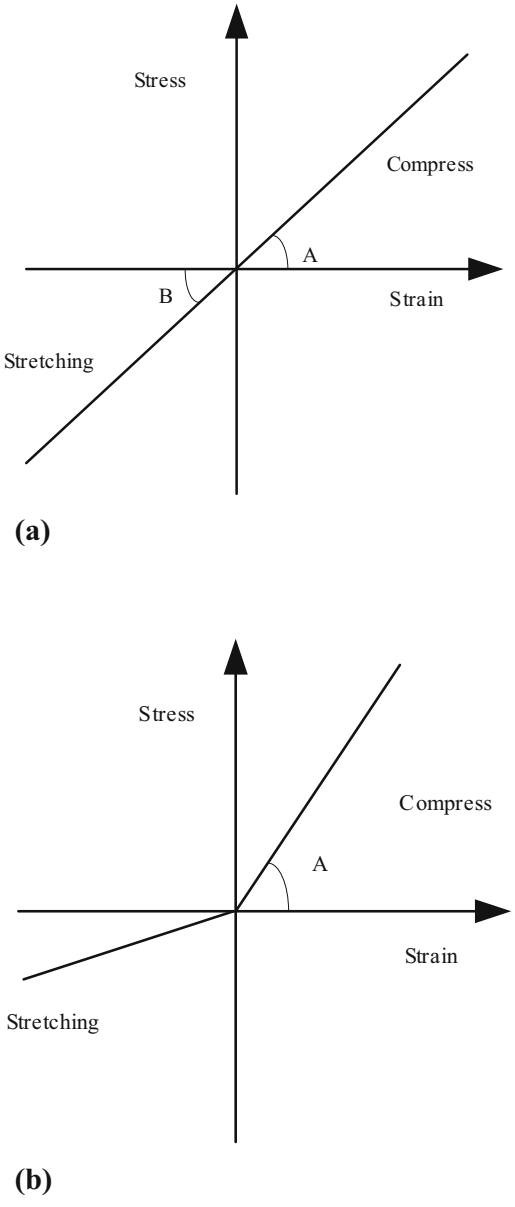

Figure 2: Vertical restoring force model of isolation bearing (a) equal tension stiffness model, (b) unequal stiffness model.

ETABS, MIDAS, etc. Although these softwares provide isolation units for seismic isolation analysis, basically it is vertically equal tensile–compression stiffness, and its restoring force model is shown in Figure 2(a). However, some literatures indicate that the model with consistent tensile and compressive stiffness is inconsistent with the actual mechanical behavior of the rubber isolation bearing, and the ratio of tensile stiffness to compressive stiffness is estimated to be between 1/4 and 1/12. Therefore, the direct use of the constitutive model provided in the software cannot reflect the true force of the isolation bearing.

After research, some scholars have proposed a parallel connection method using an isolator unit Isolator 1 and a gap unit Gap to simulate the different tensile and compressive stiffnesses of the isolated rubber bearing to ensure that the force is closer to the real situation. The Isolator 1 unit can provide both compression and tensile stiffness, while the Gap unit can provide only compression stiffness. The tensile–compression stiffness ratio of the isolated bearing defined in this paper is 1:7, and the restoring force model is shown in Figure 2(b). In Figure 2, the angle A is the compression strain angle and the angle B is the stretching angle. The unit Isolator 1 is subjected to a pressure of 1/7, the unit Gap is subjected to a pressure of 6/7, and the pulling force is fully absorbed by the unit Isolator 1, while the Gap unit does not provide tensile rigidity.

2.2.3 Seismic design

The high-rise building structure is isolated and designed by the analysis software ETABS, and the isolation is based on the base isolation. The isolation layer is arranged on the top of the basement and the floor height is 1.6 m. The top layer of the basement is used as the embedded end to adjust the arrangement of the isolation layer, and finally the isolation layer arrangement of the isolated structure is determined. A total of 45 isolated rubber bearings, including 18 lead rubber bearings and 27 laminated rubber bearings, are arranged. The mechanical performance parameters are shown in Table 4. The vertical stiffness values of the isolated bearing units under different stiffness ratios are shown in Table 5.

According to the reaction spectrum analysis, the compressive stress of the isolation bearing under gravity load (1.0 dead load + 0.5 live load) is extracted. When the tensile–compression stiffness ratio is 1:1, the maximum compressive stress of the isolation bearing is 12 MPa and the minimum value is 1.3 MPa; when the tensile–compression stiffness ratio is 1:7, the maximum compressive stress of the isolation bearing is 9 MPa and the minimum value is 0.4 MPa, which both meet the specification limit of 15 MPa; moreover, the center of gravity of the isolation layer and the center of gravity of the upper structure do not exceed 3% of the specifications.

2.2.4 Selection of seismic wave input

In order to investigate the influence of different seismic motion dimension input methods on the surface pressure of the high-rise isolated structure support, the one-, two-, and three-dimensional seismic motion modes are input to the structure, and a comparative analysis is carried out to study the influence of different dimensional seismic inputs on the performance of the isolated bearing structure.

Table 4: Mechanical properties of isolation bearings

Support model	Vertical stiffness/(kN/mm)	Equivalent damping ratio H_{eq} 100/%	Equivalent horizontal stiffness K_{eq} 100/(kN/mm)	Stiffness after yielding/(kN/mm)	Yield force/kN	Number
LRB1100	6,042	26.5	2,830	1,847	303	18
LNR1100	5,394	<5	1,806	—	—	23
LNR1300	8,532	<5	2,522	—	—	4

Table 5: Vertical stiffness of isolated isolation units with different tension–compression stiffness ratios

Tension and pressure stiffness	LRB1100/(kN/mm)		LNR1100/(kN/mm)		LNR1300/(kN/mm)	
	Isolator l	Gap	Isolator l	Gap	Isolatorl	Gap
1/1	6,042	—	8,532	—	5,394	—
1/7	863	5,179	1,219	7,313	770	4,624

3 Results

3.1 Analysis of dynamic responses of isolated structures with different aspect ratios by the velocity pulse input of near-fault seismic motion

Based on the structural model's isolation layer displacement and base shearing force as the reaction parameters, the influence of velocity pulse on the seismic response of different aspect ratio structures and the corresponding base isolation structures is analyzed. The ratio of the difference between the structural response parameters before and after the isolation to the structural response before the isolation is defined as the damping rate η_θ, which is used to reflect the damping effect of the isolation bearing.

3.1.1 Analysis of displacement of seismic isolation bearing

Table 6 shows the displacement of the isolation bearing of the base isolation structure with different aspect ratios under the action of velocity pulse seismic motion.

It can be seen from Table 6 that with the increase of the aspect ratio of the superstructure, the displacement of the isolation bearing increases first and then decreases, and reaches the maximum when H/B = 2. Figure 3 shows the correlation curve between the displacement of the seismic isolation layer and the seismic motion parameter V_{max}/A_{max} of the base isolation structure under the action of six seismic motion inputs. By linearly fitting the results, it can be seen more intuitively that the displacement of the isolation bearing increases with the increase of V_{max}/A_{max} (except when the structural aspect ratio is 1, the directional effect of velocity pulse seismic motion A2 acts).

Under the action of seismic motion B1, when H/B is 1, 2, and 3, the displacement of the isolation bearing exceeds the bearing displacement limit (0.33 m); especially when H/B = 2, the displacement of the isolation bearing has reached 0.61 m, which will cause serious damage to the isolation bearing.

Table 6: Displacement of isolation bearings with different aspect ratio structures

Seismic number	δ/m			
	H/B = 1	H/B = 2	H/B = 3	H/B = 4
A1	0.2855	0.3262	0.2225	0.1261
A2	0.1982	0.3251	0.2602	0.1619
A3	0.212	0.2777	0.2028	0.1049
B1	0.3536	0.6141	0.5723	0.1988
B2	0.1401	0.3146	0.2743	0.1292
B3	0.0745	0.1292	0.1183	0.1021

3.1.2 Analysis of the base shearing force

In order to better reflect the influence of the seismic motion velocity pulse on the base isolation effect of different aspect ratio structures, the maximum base shearing force before and after the structural isolation is taken as the analysis parameter, and the maximum base shearing force before and after the structural isolation is calculated, as shown in Figure 4, and the damping rate of the base shearing force is calculated, as shown in Table 7.

It can be seen from Figure 4 and Table 7 that the maximum base shearing force increases with the increase of the aspect ratio, and the isolation bearing has a certain isolation effect on the maximum base shearing force of the structure. However, as the aspect ratio of the superstructure increases, the damping rate gradually decreases. At the same time, it can be seen that the influence of seismic motion velocity pulse on the maximum base shearing force of the structure is similar to the effect on the displacement angle between layers.

3.2 Analysis of the influence of different dimensional vibration input methods on the isolation bearing under unequal tensile–compression stiffness ratio

The seismic motion analysis method of inputting different dimensionalities and the isolation structure with different stiffness ratios is conducted using the time-history analysis of rare earthquakes, and the variation and law of the surface pressure of each bearing are studied to obtain different dimensions, to obtain the influence of the seismic motion mode input on the performance of the isolated structure under different seismic conditions. When checking the tensile stress of the isolation bearing, the load combination value is calculated by equation (1). When the compressive stress

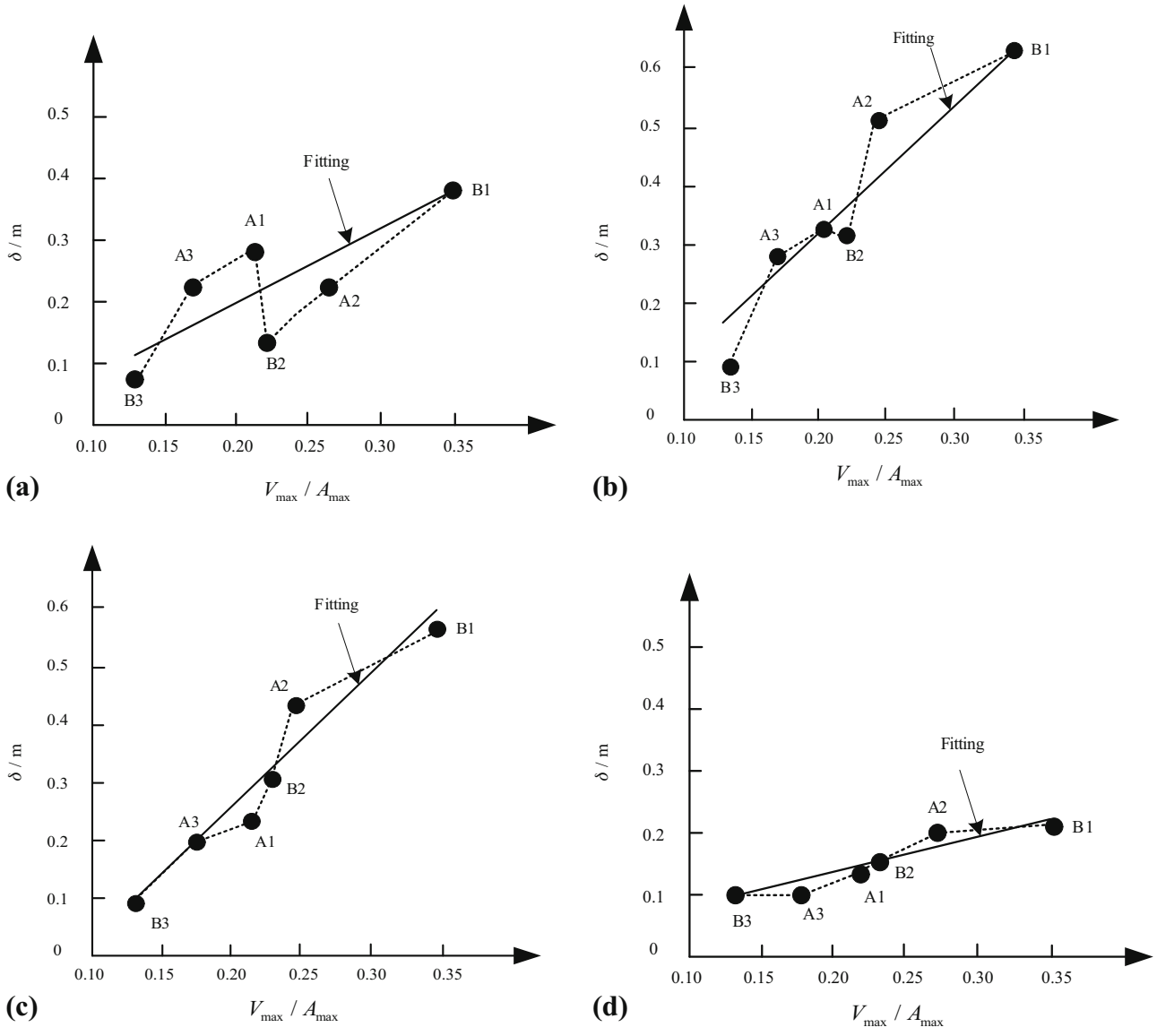

Figure 3: Displacement of isolation bearings with different aspect ratio structures under different vibration input modes (a) H/B = 1. (b) H/B = 2. (c) H/B = 3. (d) H/B = 4.

of the isolation bearing is checked, the load combination is calculated by equation (2):

$$C_1 = \frac{1.0 \text{ constant load} + 0.5 \text{ live load} + 1.3 \text{ minimum axial force generated by earthquake forces}}{S} \quad (1)$$

$$C_2 = \frac{1.2 \text{ constant load} + 0.6 \text{ live load} + 1.3 \text{ maximum axial force generated by earthquake forces}}{S} \quad (2)$$

where C_1 indicates the load combination value when checking the tensile stress of the isolation bearing and C_2 indicates the load combination value when checking the compressive stress of the isolation bearing; S indicates the area of the isolation bearing; the axial force generated by the seismic force is the average value of the seven sets of seismic waves.

Taking the tensile–compression stiffness ratio of the isolation unit as the quantitative, and the tensile–compression stiffness ratio as 1:7, the difference in the surface pressure of the isolation bearing under different dimensional seismic motion inputs is compared and

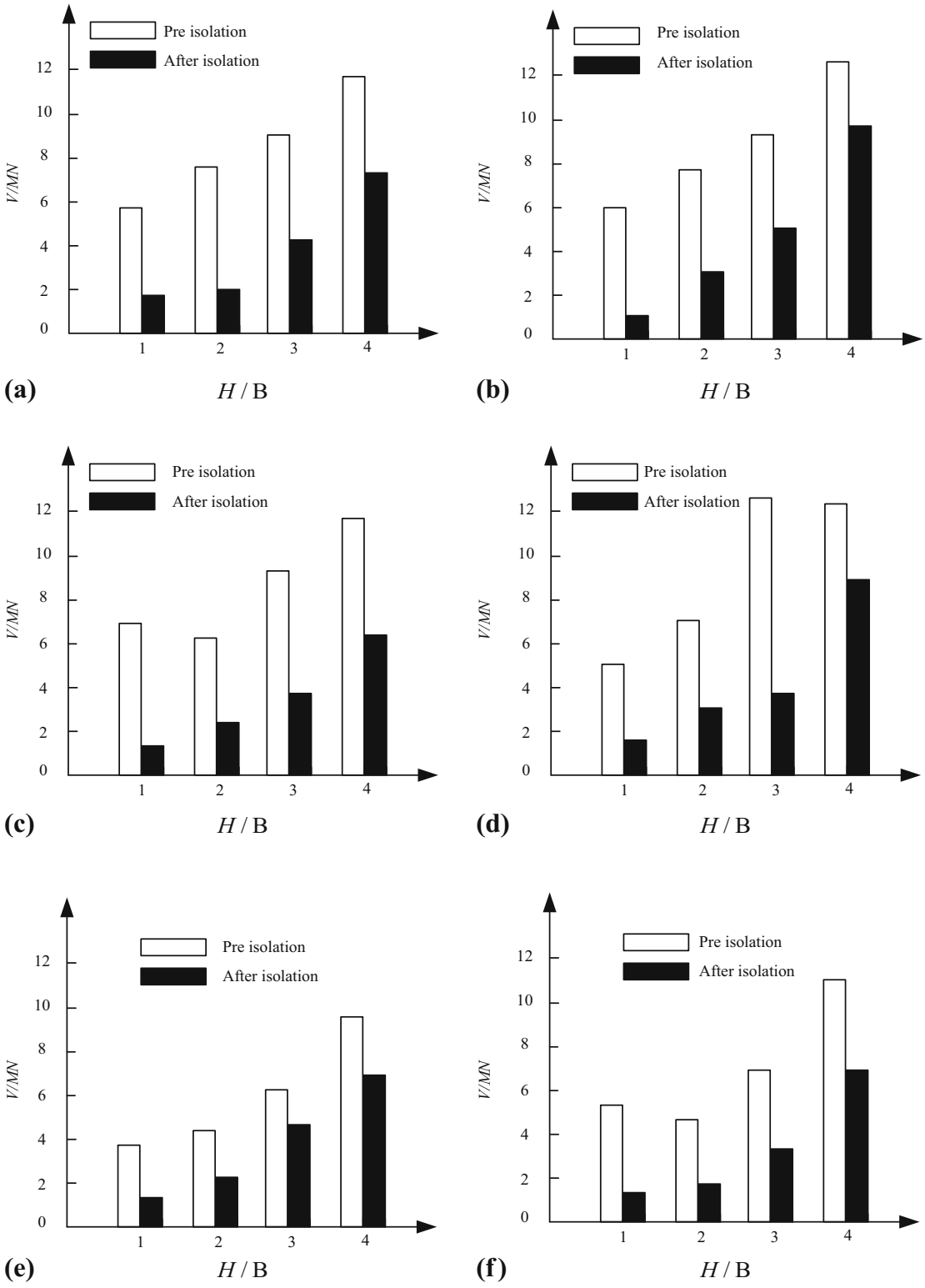

Figure 4: Maximum base shear of non-isolated and isolated structures with different aspect ratios: (a) seismic motion A1, (b) seismic motion A2, (c) seismic motion A3, (d) seismic motion B1, (e) seismic motion B2, (f) seismic motion B3.

Table 7: Maximum base shear rate of structures with different aspect ratios

Seismic number	η_v			
	H/B = 1	H/B = 2	H/B = 3	H/B = 4
A1	0.7	0.703	0.541	0.352
A2	0.635	0.591	0.403	0.14
A3	0.794	0.648	0.544	0.441
B1	0.66	0.563	0.52	0.305
B2	0.675	0.52	0.285	0.323
B3	0.78	0.652	0.53	0.381

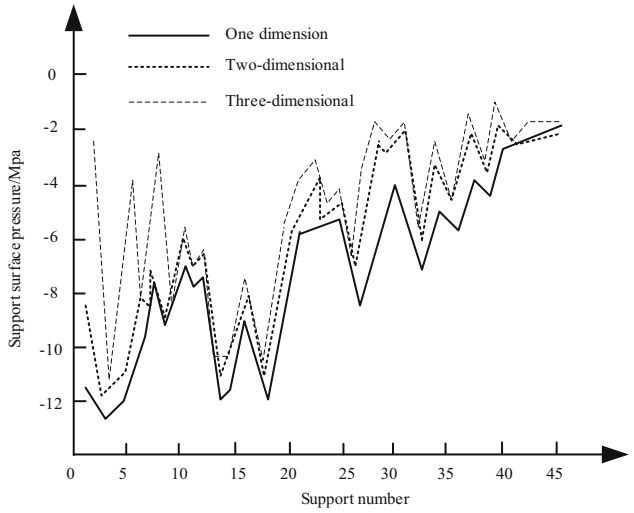

Figure 5: *X* tensile stress of the isolation support.

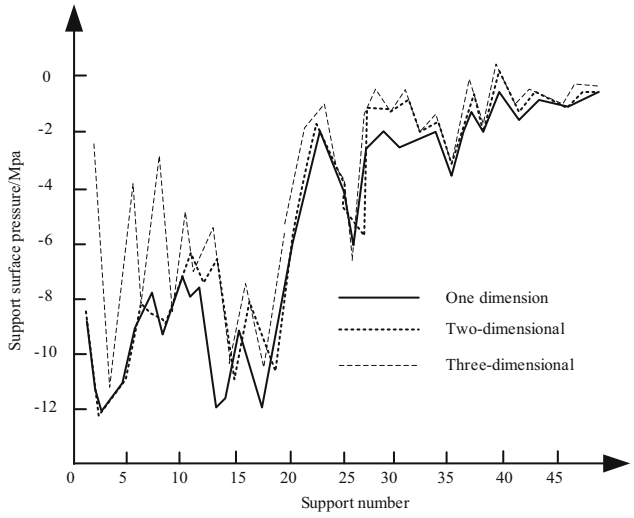

Figure 6: *Y*-Direction tensile stress of the isolation support.

analyzed. The analysis results are shown in Figures 5–8. As shown, positive values in the figures indicate tensile stress and negative values indicate compressive stress.

It can be seen from Figures 5–8 that the surface pressure of the isolation bearing changes under different dimensional seismic motion inputs. For the tensile stress of the isolation bearing, only the surface pressure of a small part of the isolation bearing has a large variation, and the surface pressure of most of the isolation bearing has only a small change.

4 Discussion

4.1 Discussion on the influence of near-fault seismic motion velocity pulse input on the performance of different aspect ratio isolation structures

4.1.1 Discussion on the displacement of the isolation bearing

Analysis of Table 6 shows that with the increase of the aspect ratio of the superstructure, the displacement of the isolation bearing increases first and then decreases. When H/B = 2, the maximum value is obtained. Through the correlation curve between the displacement of the isolation layer and the seismic motion parameter V_{max}/A_{max} of the base isolation structure under the action of the six seismic motion inputs described in Figure 3, the results are linearly fitted, which can be more intuitively seen that the displacement of the isolation bearing increases with the increase of V_{max}/A_{max}, except when the structural aspect ratio is 1, the directional effect of velocity pulse seismic motion A2 acts. In the B1 vibration input mode, when the H/B value is 1, 2, and 3, the displacement of the isolation bearing exceeds the displacement limit of the bearing. It is worth noting that when H/B = 2, the displacement of the isolation bearing reaches 0. 61 m, and it is extremely prone to cause severe damage to the isolation bearing. Therefore, in the design of the base isolation structure in the near-field fortification zone, the velocity pulse characteristics of the seismic motion to make the displacement of the seismic isolation bearing overrun should be prevented, and appropriate measures should be taken to limit the displacement of the structural bottom layer or to strengthen the design of the isolation bearing.

In summary, under the action of the near-fault velocity pulse type of seismic motion, with the increase of the aspect ratio H/B (taking 1–4), the maximum shearing force of the structural base increases gradually, but the displacement of the isolation bearing has a tendency of increasing first and then decreasing, and as the V_{max}/A_{max} value of seismic motion increases, the

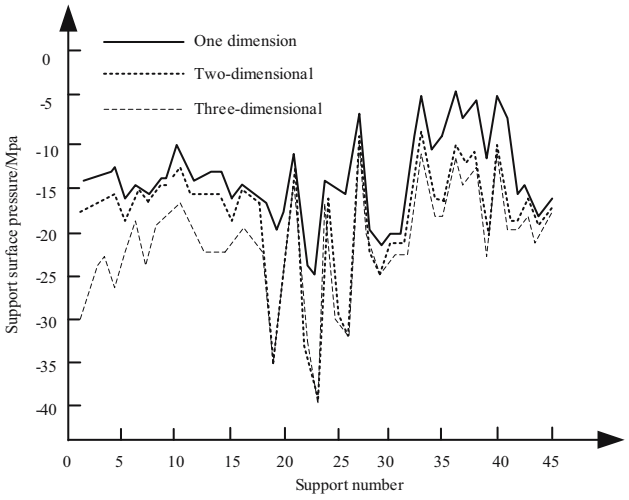

Figure 7: X-ray compressive stress of the isolation support.

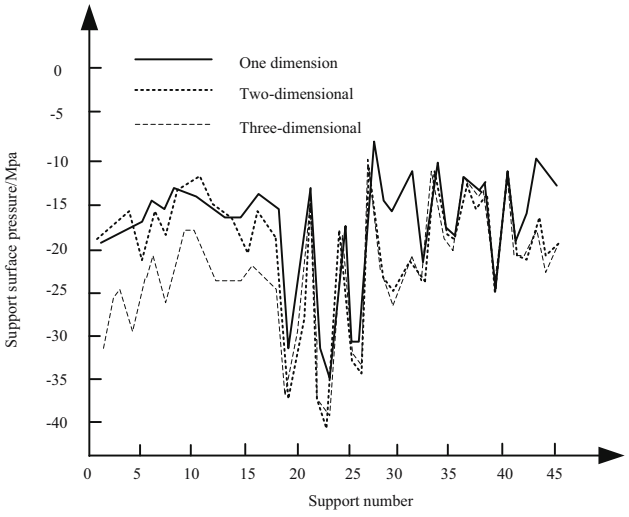

Figure 8: *Y*-Direction compressive stress of the isolation support.

displacement of the isolation bearing also gradually increases.

4.1.2 Discussion on the base shearing force

Analysis of Figure 4 and Table 7 shows that the maximum base shearing force increases with the increase of the aspect ratio, and the isolation bearing has a certain isolation effect on the maximum base shearing force of the structure. However, with the increase of the aspect ratio of the superstructure, the damping rate is gradually reduced, that is, the structural isolation performance of H/B = 1 is the best, and the isolation performance of H/B = 4 structure is the worst. In addition, the influence of the seismic motion velocity pulse on the maximum base shearing force of the structure is similar to the effect on the interlayer displacement angle.

Therefore, for a structure with an aspect ratio H/B of 1, 2, and 3, the base isolation has a good damping effect, and the smaller the aspect ratio is, the better the damping effect is. When the structure H/B = 4, the effect of the base isolation is poor, and the isolation structure may be destroyed due to the excessive displacement of the lower structure or the isolation bearing.

4.2 Discussion on the influence of different dimensional seismic motion input methods on the isolation performance of seismic isolation bearings

It can be seen from the analysis of Figures 5–8 that the surface pressure of the seismic isolation mount changes under different dimensional seismic motion inputs. For the tensile stress of the isolation bearing, only the surface pressure of a small part of the isolation bearing has a large variation, and the surface pressure of most of the isolation bearing has only a small change. From the numerical value, the one-dimensional seismic motion input is the smallest, the two-dimensional seismic motion input is next, and the maximum is three-dimensional seismic motion input, with the maximum value of 12.1 MPa. For the compressive stress of the isolation bearing, the variation of the surface pressure of most isolated bearings is still relatively large. From the numerical value, the one-dimensional seismic motion input is the smallest, the two-dimensional seismic motion input is next, and the maximum is three-dimensional seismic motion input, with the maximum value of 40.4 MPa. This shows that when the tensile–compression stiffness ratio of the isolation unit is 1:7, the seismic motion input of different dimensions still affects the surface pressure of the isolation bearing, but the impact is slightly reduced.

Under the same dimensional seismic motion input, the tensile–compression stiffness ratio has a greater influence on the tensile stress of the isolation bearing, but has little effect on the compressive stress. This shows that the tensile–compression stiffness ratio also affects the surface pressure of the isolation bearing.

5 Conclusions

In this paper, different vibration input methods are used to test the impact of seismic isolation performance on

different seismic measures, and the following conclusions are drawn:

By studying the influence of the pulse input of the near-fault seismic motion velocity on the isolation performance of the base-isolated structures with different aspect ratios, it can be seen that for the structure with the aspect ratio H/B of 1, 2, and 3, the base isolation has a better damping effect. And the smaller the aspect ratio is, the better the damping effect is. When the structure H/B = 4, the effect of the base isolation is poor, and even the displacement of the lower layer or the isolation bearing is too large, the isolated structure is damaged.

Through the study of the influence of different dimensional seismic motion input methods on the isolation performance of the isolation bearing, it can be known that when the tensile–compression stiffness ratio of the isolation unit is 1:7, the seismic motion input of different dimensions will still affect the surface pressure of the isolation bearings, but the influence is slightly reduced. Therefore, the vibration input of different dimensions has an influence on the isolation performance of the isolation bearing, but the influence is small. From small to large, they are: one-dimensional vibration input, two-dimensional vibration input, and three-dimensional vibration input.

Based on the above conclusions, it is suggested that in the near-fault zone for a strong earthquake, the frame structure with the aspect ratio H/B greater than 3 should avoid the use of a basic isolation design or adopt a design scheme that fully considers the adverse effects of the seismic motion velocity pulse. At the same time, in the design of the base isolation structure of the near-fault zone for a strong earthquake, appropriate measures should be taken to limit the displacement of the bottom layer of the structure or to strengthen the design of the isolation bearing.

Acknowledgments: This research was supported by the Science and Technology Project of Guangzhou (No. 201707010333) and National Natural Science Foundation Youth Fund of China (No. 51808467).

References

[1] Castaldo P, Tubaldi E. Influence of FPS bearing properties on the seismic performance of base-isolated structures. Earthquake Eng Struct Dyn. 2015;44(15):2817–36.
[2] Zhan CB, Luo C, Ding ZK, Jin XL. Research on seismic performance prediction of high-rise buildings. Comput Simul. 2016;33(8):397–402.
[3] Li Z, Han C, Wei D. Empirical research on the relationship between natural gas consumption and economic growth in the northeast Asia. Energy Environ. 2018;29(2):216–31.
[4] Liu Z. Economic analysis of energy production from coal/biomass upgrading; part 1: hydrogen production. Energy Sources Part B Econ Plan Policy. 2018;13(2):132–6.
[5] Peng W, Ge S, Ebadi AG, Hisoriev H, Esfahani MJ. Syngas production by catalytic co-gasification of coal-biomass blends in a circulating fluidized bed gasifier. J Cleaner Product. 2017;168:1513–17.
[6] Li Y, Conte JP. Effects of seismic isolation on the seismic response of a California high-speed rail prototype bridge with soil-structure and track-structure interactions. Earthquake Eng Struct Dyn. 2016;45(15):2415–34.
[7] Monzon EV, Buckle IG, Itani AM. Seismic performance and response of seismically isolated curved steel I-girder bridge. J Struct Eng. 2016;142(12):04016121.
[8] Siringoringo DM, Fujino Y. Long-term seismic monitoring of base-isolated building with emphasis on serviceability assessment. Earthquake Eng Struct Dyn. 2015;44(4):637–55.
[9] Ahmadi A, Kunnath SK, Abrahamson N. Influence of dominant response modes on structural seismic demand modeling. J Struct Eng. 2016;142(1):04015093.
[10] Xuan S, Gao Q. Novel integrated battery charger based on a four-switch inverter for electric vehicles. J Power Supply. 2017;5(2):122–298.
[11] Ashour A, El-Dakhakhni W. Influence of floor Diaphragm–Wall coupling on the system-level seismic performance of an asymmetrical reinforced concrete block building. J Struct Eng. 2016;142(10):04016071.
[12] Fathipour V, Jang SJ, Nia IH, Mohseni H. Impact of three-dimensional geometry on the performance of isolated electron-injection infrared detectors. Appl Phys Lett. 2015;106(2):021116.
[13] Zhang NT, Zhao KL, Liu GL. Thought on constructing the integrated space-terrestrial information network. J China Acad Electron Inform Technol. 2015;3(12):455–687.
[14] Roeder CW, Lehman DE, Clark K, Powell J,Yoo JH,Tsai KC, et al. Influence of gusset plate connections and braces on the seismic performance of X-braced frames. Earthquake Eng Struct Dyn. 2015;40(4):355–74.
[15] Malhotra PK. Dynamics of seismic impacts in base-isolated buildings. Earthquake Eng Struct Dyn. 2015;26(8):797–813.
[16] Adam M, Assimakis N. Kstep fibonacci sequences and fibonacci matrices. J Discrete Math Sci Cryptogr. 2017;20(5):1183–206.
[17] Chande MK, Lee C, Li C. Cryptanalysis and improvement of a ECDLP based proxy blind signature scheme. J Discrete Math Sci Cryptogr. 2018;21(1):23–34.
[18] Korpinar T, Turhan E. Inextensible flows of biharmonic s-curves according to sabban frame in Heisenberg group HEIS3. J Interdiscipl Math. 2018;21(1):17–27.
[19] Malangone P, Ferraioli M. A modal procedure for seismic analysis of non-linear base-isolated multistorey structures. Earthquake Eng Struct Dynam. 2015;27(4):397-412.
[20] Song SX, Pan YS, Long X, Zhou Y. Construction of earthquake disaster prevention system for high speed railway. Automat Instrum. 2015;6(4):198–322.
[21] Makris N, Chang S. Effect of viscous, viscoplastic and friction damping on the response of seismic isolated structures. Earthquake Eng Struct Dyn. 2015;29(1):85–107.